5-2020

Development of an In Vitro Intervertebral Disc Innervation Model to Screen Neuroinhibitory Biomaterials

Sarah M. Romereim

Caleb A. Johnston

Adan L. Redwine,

Rebecca A. Wachs

HHS Public Access

Author manuscript

J Orthop Res. Author manuscript; available in PMC 2020 May 22.

Published in final edited form as:

J Orthop Res. 2020 May ; 38(5): 1016–1026. doi:10.1002/jor.24557.

Development of an In Vitro Intervertebral Disc Innervation Model to Screen Neuroinhibitory Biomaterials

Sarah M. Romereim, **Caleb A. Johnston**, **Adan L. Redwine**, **Rebecca A. Wachs**

Biological Systems Engineering, University of Nebraska-Lincoln, P.O. Box 830726, Lincoln, Nebraska, 68583-0726

Abstract

Pain originating from an intervertebral disc (discogenic pain) is a major source of chronic low back pain. Pathological innervation of the disc by pain-sensing nerve fibers is thought to be a key component of discogenic pain, so treatment with biomaterials that have the ability to inhibit neurite growth will greatly benefit novel disc therapeutics. Currently, disc therapeutic biomaterials are rarely screened for their ability to modulate nerve growth, mainly due to a lack of models to screen neuromodulation. To address this deficit, our lab has engineered a three dimensional in vitro disc innervation model that mimics the interface between primary sensory nerves and the intervertebral disc. Further, herein we have demonstrated the utility of this model to screen the efficacy of chondroitin sulfate biomaterials to inhibit nerve fiber invasion into the model disc. Biomaterials containing chondroitin-4-sulfate (CS-A) decrease neurite growth in a uniform gel and at an interface between a growth-permissive and a growth-inhibitory gel, while chondroitin-6-sulfate (CS-C) is less neuroinhibitory. This in vitro model holds great potential for screening inhibitors of nerve fiber growth to further improve intervertebral disc replacements and therapeutics.

Keywords

low back pain; intervertebral disc; discogenic pain; chondroitin sulfate; neuroinhibition

Chronic low back pain (LBP) is a major cause of disability, healthcare costs, and decreased quality of life.[1,2] All age groups are affected by chronic LBP, and it is a global epidemic with a lifetime prevalence of 38.9% and increased severity in older populations.[3,4] An estimated 26–42% of chronic LBP cases are due to pain originating within the intervertebral disc, which is termed disc-associated or discogenic LBP.[5–7] Current treatments for discogenic pain include long-term pain medication, physical therapy, semi-invasive treatments such as anti-inflammatory injections, and surgeries such as spinal fusions;

Correspondence to: Rebecca A. Wachs (T: 402 472-2262; F: 402-472-6338; rebecca.wachs@unl.edu).

AUTHORS' CONTRIBUTION

S.M.R. performed the experiments described and wrote the manuscript with guidance and feedback from R.A.W. and proofreading by C.A.J. and A.L.R. Data analysis was performed by S.M.R., C.A.J., A.L.R., and R.A.W. Statistical analysis was performed by S.M.R. Funding for the study was obtained by R.A.W. All authors have read and approved the submitted manuscript.

Conflicts of interest: None.

SUPPORTING INFORMATION

Additional supporting information may be found in the online version of this article.

however, these options have limited efficacy for most patients.[8–11] Therefore, alternative treatments for chronic discogenic LBP are needed.

Developing new treatments for discogenic LBP requires a mechanistic understanding of its causes, which are closely tied to changes in the disc that occur during disc degeneration. The disc is composed of an outer lamellar ring, the annulus fibrosus (AF), and an inner core called the nucleus pulposus (NP). The NP contains high amounts of chondroitin sulfate proteoglycans (CSPGs) such as aggrecan that maintain the water content of the disc and inhibit nerve growth and vascularization.[12,13] The healthy disc is predominantly aneural and avascular, with nerve fibers (i.e., neurites) and blood vessels limited to the outer edges of the AF. During disc degeneration, the matrix of the disc degrades and the concentration of CSPGs decreases, the disc loses water content and height, and other disruptions such as annular fissures occur.[8,14] The reduction in CSPG-rich neuroinhibitory matrix combines with degenerate disc cell secretion of neurotrophic factors (e.g., NGF and BDNF) and proangiogenic factors (e.g., VEGF) to promote sensory neurite and blood vessel growth into the disc.[8,15,16] Once the disc has become innervated with pain-sensing (nociceptive) neurites, the nerve endings may be directly stimulated by inflammatory factors, irritants, or growth factors secreted by disc cells.[8,15] Sensory neurites stimulated by the harsh microenvironment within the degenerate disc are the proposed source of discogenic pain.[8,15]

Clinical evidence from patients with disc degeneration and LBP further supports the role of disc innervation in discogenic pain. For example, in one study 68% of 61 human degenerate discs were innervated.[17] Many researchers have found evidence of nociceptive neurite markers deep within discs (sometimes extending into the NP) of patients with LBP.[18–22] Specifically, markers of pain sensation such as substance P and calcitonin gene-related peptide (CGRP) are found in the majority of the neurites identified in degenerate, painful discs.[22] Additionally, recent evidence of innervation in discogenic neck pain supports a similar mechanism for discogenic LBP.[23,24] Induced and age-related disc degeneration in mouse and rat models have also exhibited increased disc innervation, including into the NP.[25–28] These data demonstrate a strong link between disc degeneration, increased disc innervation, and discogenic pain.

Despite the strong association between disc innervation and discogenic pain, current biomaterials for disc regeneration are often characterized with the disc environment in mind but without direct examination of the effects on sensory neurite growth.[29,30] This is due to a lack of in vitro models that mimic the conditions of pathological disc innervation where sensory nerves sprout through the AF into the NP. Current models of neuroinhibition often utilize two-dimensional (2D) cultures of sensory neurons on a neuroinhibitory substrate[12,31,32] or single component hydrogels[33] which do not adequately mimic the complex disc environment. Previous in vitro research of the behavior of neurites at a 3D interface was limited to a glial scar model utilizing embryonic chick dorsal root ganglia (DRG), which is not representative of pathologic disc innervation because the gel contents are not similar to the disc.[34] Here, we present a novel model that mimics pathologic innervation in the disc by creating an interface between a nerve growth-permissive hydrogel and a disc-like gel to screen neuroinhibitory properties of specific materials (Fig. 1).

The initial candidate materials chosen for assessment with our in vitro disc innervation model were chondroitin sulfate (CS) biomaterials as there is a robust connection between increased disc innervation and the reduction of neuroinhibitory CSPGs that occurs with age and disc degeneration.[12,13,35] The neuroinhibitory properties of CSPGs are determined by the different sulfation patterns of the CS the CSPGs contain because the sulfation pattern determines the neuronal receptors to which the CS can bind.[36–38] In bovine aggrecan, the main sulfation patterns are 62.3% chondroitin-4-sulfate (CS-A; Fig. 1A), 25% chondroitin-6-sulfate (CS-C; Fig. 1B), and 12.7% unsulfated chondroitin.[33] Human aggrecan from articular sources also consists mainly of CS-A and CS-C, with the ratio between the two varying with age and location in the tissue.[39] Interestingly, the effects of CS-A and CS-C can range from strongly neuroinhibitory to not neuroinhibitory at all depending on the species and neuronal cell type investigated (mouse, rat, or chicken; cerebellar granule neuron, cortical neuron, or DRG neuron).[31,33,34,40,41] To maximize relevance to disc physiology, CS-A and CS-C were chosen as potential neuroinhibitory biomaterials for screening in our model.

The goals of this work were to (i) engineer a culture model to mimic sensory neurite growth into an intervertebral disc and (ii) screen CS biomaterials for rat DRG neuroinhibition. The hypothesis of this study was that CS-A and CS-C would inhibit neurite growth of neonatal rat DRGs in hydrogel culture. The neuroinhibitory properties of CS-A and CS-C biomaterials were first assessed in 3D uniform composition hydrogels, demonstrating that CS-A was more strongly neuroinhibitory than CS-C. The in vitro disc innervation model assessing neuroinhibition at the interface of two different gels then established that CS-A is neuroinhibitory at an interface, and enzymatic digestion of the CS-A significantly decreased the neuroinhibition thereby verifying that CS is necessary for neuroinhibition. Together, these results demonstrate we have established an in vitro innervation model capable of screening neuroinhibitory properties of biomaterials and that CS-A is an effective neuroinhibitory biomaterial with potential uses in disc biomaterials.

METHODS

Fabrication and Characterization of Methacrylated Biomaterials

Biomaterial Synthesis—Hyaluronic acid (HA, 53747; MilliporeSigma, St. Louis, MO) was the control scaffold because HA is prevalent in disc extracellular matrix and does not modulate neurite growth. Chondroitin sulfate A from bovine trachea (CS-A, C6737; MilliporeSigma) and chondroitin sulfate C from shark cartilage (C4384; MilliporeSigma) were the neuroinhibitory molecules screened (Fig. 1A and B). Methacrylic anhydride (276685; MilliporeSigma) groups were added to the backbone molecules (HA, CS-A, or CS-C) according to published methods[42,43] to permit UV-photo- initiated polymerization of the methacrylated biomaterials (designated by MA prefix) MAHA, MACS-A, or MACS-C (Fig. 1D). Methacrylation: 0.5 g HA, 2.5 g CS-A, or 2.5 g CS-C in ultrapure water reacted with excess MA (1.895 ml for HA, 10 ml for CS-A or CS-C) at 4°C with NaOH pH adjustment to 8. Each compound was precipitated twice in ethanol (MAHA) or once in acetone (MACS-A, MACS-C), dialyzed for 3 days using a 10 MW cassette (87733; Thermo

Fisher Scientific, Waltham, MA), and lyophilized (710401000; Labconco, Kansas City, MO).

Nuclear Magnetic Resonance (NMR) Spectroscopy Characterization of Biomaterials—NMR was used to characterize the degree of methacrylation. Samples were dissolved in deuterium oxide (1133660100; MilliporeSigma) at 2 mg/ml for MAHA and 10 mg/ml for MACS-A and MACS-C. Proton NMR spectroscopy was performed (Avance III-HD 700 MHz spectrometer; Bruker, Billerica, MA) in the University of Nebraska-Lincoln Research Instrumentation Facility. Degree of methacrylation was the ratio of the methacrylate peak integral at ~1.8 ppm to the HA/CS carbohydrate peak integral at ~1.9 ppm.[42,44] The NMR peaks created by methacrylation were identified by comparison with the NMR spectra for unmethacrylated HA/CS (data not shown) and also by referencing published peak locations.[42,44]

Base Hydrogel Composition

All culture experiments utilized the following biomaterial combinations: (i) MAHA at 2.50 mg/ml, (ii) MAHA at 2.25 mg/ml plus MACS-A at 10 mg/ml, or (iii) MAHA at 2.25 mg/ml plus MACS-C at 10 mg/ml. All hydrogels contained the following components: type I collagen at 2.25 mg/ml, 0.3% Irgacure (2-Hydroxy-4′ (2-hydroxyethoxy)-2-methylpropiophenone; 410896; MilliporeSigma), 1× DMEM (D2429; MilliporeSigma), 250 mM HEPES (H0887; MilliporeSigma), and 138 mM sodium bicarbonate (S6014; MilliporeSigma). First, Irgacure was dissolved in concentrated DMEM/HEPES/sodium bicarbonate solution, and then methacrylated biomaterials (MAHA, MACS-A, and MACS-C) were added and dissolved for 2 days at room temperature in the dark with agitation. The day of gel fabrication, 1× phosphate-buffered saline (PBS) and type I collagen (354249; Corning Inc., Corning, NY) were added on ice.

Mechanical Characterization

The base hydrogel mixtures were injected from a syringe with a 23-gauge needle into an 8 mm diameter silicone mold (666305; Grace BioLabs, Bend, OR) sandwiched between glass slides. Slides were then subjected to thermal gelation for 30 min at 37°C followed by 2.5 min of UV-photo-initiated cross-linking on each side of the mold. Hydrogels were removed from the molds and kept in 1× PBS overnight at 4°C before rheology. Porcine NP tissue punches (8 mm diameter) were also characterized. Porcine cervical spines were obtained through a material transfer agreement with the United States Meat Animal Research Center (USMARC, USDA ARS). Intact NPs were isolated and a punch biopsy tool (501181245; Thermo Fisher Scientific) used to create a cylinder of NP tissue. Viscoelastic properties (storage and loss moduli) of the hydrogel samples and NP tissue punches were measured using oscillatory rheology with a frequency sweep from 0.1 to 1.0 rad/s on a rheometer (MCR 302; Anton Paar, Graz, Austria).

Cytocompatibility of Hydrogels with NP Cells

Human NP Cell Culture—Commercially available human NP cells (4800; ScienCell, Carlsbad, CA) were expanded in complete NP media (4801; ScienCell) in a T75 flask coated with poly-L-lysine (413; Scien-Cell) at 37°C in hypoxic conditions (3.5% O_2, 10% CO_2,

86.5% N_2) using a hypoxia chamber (27310; StemCell Technologies, Vancouver, Canada). After expansion, cells were trypsinized (25200056; Thermo Fisher Scientific), counted, and resuspended in cold 1× PBS for incorporation into hydrogels at a seeding density of 1.5 million cells/ml. Cells were mixed with the base hydrogel described above, and 150 μl pipetted into 48-well plate prior to thermal gelation (30 min at 37°C) followed by UV-photo-initiated cross-linking (90 s). Gels were cultured with 300 μl complete NP media at 37°C in normoxic conditions.

Metabolic Activity Assessment—NP cell populations embedded in hydrogels were evaluated using an alamarBlue assay (88951; Thermo Fisher Scientific) according to the manufacturer's instructions on days 1, 4, and 7 of culture. Media absorbance at 570 and 600 nm was measured using a microplate reader (Synergy H1; BioTek, Winooski, VT) and the percent of alamarBlue reduction calculated.

Cell Viability—At the end of 7 days of culture, the proportion of living and dead NP cells in selected samples were determined using a LIVE/DEAD® Viability/Cytotoxicity Kit (L3224; Thermo Fisher Scientific) according to manufacturer's instructions with 2 μM calcein AM and 4 μM EthD-1 for 20–30 min. Cells were imaged on a confocal laser scanning microscope (LSM 800; Carl Zeiss Microimaging, Inc., Jena, Germany) on a single plane 60 μm below the gel surface at three distinct x–y locations in each gel using excitation at 488 nm for calcein AM and 561 nm for EthD-1. Quantification was performed using the Zen Blue 3.0 Image Analysis software (Carl Zeiss Microimaging, Inc.).

Dorsal Root Ganglion Culture

Neonatal Rat DRGs—All animal experiments were performed in accordance with the Guide for the Care and Use of Laboratory Animals and approved through the University of Nebraska-Lincoln's Institutional Animal Care and Use Committee. Sprague–Dawley rats aged postnatal days 0–3 were euthanized and DRGs were removed by sterile dissection (Fig. 1C), placed in cold Neurobasal media (21103049; Thermo Fisher Scientific), nerve roots trimmed to remove all pre-existing neurites outside of the DRG, and body of the DRG cut into two pieces prior to hydrogel embedding a single DRG piece per gel. For larger DRGs, both halves were embedded separately, and for smaller DRGs the cut was made so that one piece was larger (and approximately equal in size to each half of the large DRGs).

Culture Conditions—DRG hydrogel cultures used 300 μl complete media per well and were cultured for 5–7 days at 37°C with 5% CO_2 in normoxia. The complete DRG media was Neurobasal media (21103049; Thermo Fisher Scientific) supplemented with 10% FBS, 1% penicillin/streptomycin, 1% GlutaMax (35050-061; Thermo Fisher Scientific), 1% B27 (17–504-044; Thermo Fisher Scientific), and 0.01% NGF (556-NG-100; R&D Systems, Minneapolis, MN).

Determination of Neuroinhibition in Uniform 3D Hydrogels

Hydrogel mixtures were prepared as described in the Base Hydrogel Composition section with the addition of 0.75 mg/ml laminin (344600501; R&D Systems) to enhance DRG cell attachment. Neuroinhibitory properties of CS biomaterials were initially assessed in uniform

composition 3D hydrogels. To make the hydrogels, 150 μl of the hydrogel mixture was pipetted into a well of a 48-well plate, a trimmed DRG embedded, and then thermal gelation (30 min at 37°C) followed by UV-photo-initiated cross-linking (90 s) performed (Fig. 1D). Samples were cultured for 5 days followed by neurite quantification (see section below).

Development and Characterization of the In Vitro Disc Innervation Culture Model

The disc innervation model featured an inner gel core to screen neuroinhibition of specific biomaterials (MACS-A and MACS-C) and an outer neuro-permissive gel to embed the DRG. To create the inner hydrogel, 100 μl of gel mixture was pipetted into a well of a 96-well plate on top of a polypropylene sheet with handles to enable lifting the gel from the well after thermal gelation (20 min at 37°C). The inner gel was then transferred to a 48-well plate, and 150 μl of the outer gel mixture pipetted into the adjacent area. A trimmed DRG was placed near the interface of the two gels, and the outer gel was thermally (20 min at 37°C) and UV cross-linked (90 s), followed by culture for 7 days and neurite quantification (Fig. 1D).

Specific enzymatic digestion of CS in the inner gel was performed to verify the mechanism of neuroinhibition. MAHA and MACS-A inner gels were made as above; however, both thermal (30 min at 37°C) and UV cross-linking (90 s) were performed immediately. Gels were washed with HBSS (BW10–543F; Thermo Fisher Scientific), incubated with 2.5U chondroitinase ABC (C3667; MilliporeSigma) in 2 ml HBSS plus 61 mM sodium acetate (W302406; MilliporeSigma) for 3 h at 37°C, and washed 9× 15 min with PBS before being stored in PBS at 4°C overnight. Then outer gel fabrication, DRG embedding, and culture for 7 days were performed as with the disc innervation model, followed by neurite quantification.

Neurite Quantification

DRG hydrogels were fixed for 1–2 h with 4% PFA, washed with 1× PBS, blocked with 1× PBS containing 4% goat serum (G9023; MilliporeSigma) and 0.5% Triton X-100 (93443; MilliporeSigma) for 1–2 h at room temperature, and incubated with blocking buffer containing anti-Neurofilament-H antibody (RT97; University of Iowa Developmental Studies Hybridoma Bank) at 0.45 μg/ml for 36 h at 4°C. Neurofilament H is a component of the intermediate filament of the neuronal cytoskeleton and is used to visualize neuronal morphology. Three 4-h room temperature washes with PBST (1× PBS plus 0.05% Tween-20; BP337-100; Thermo Fisher Scientific) were followed by a 12-h incubation with blocking buffer containing goat anti-mouse Alexafluor 488 antibody (ab150117; Abcam, Cambridge, MA). Finally, three 4-h washes with PBST, 20 min incubation with 1 μg/ml DAPI in PBS and three 15-min PBS washes. Imaging was performed on either (i) a confocal LSM 800 microscope or (ii) a cell imaging plate reader (Cytation 1; BioTek). Neurite length was measured by one to two blinded observers from the maximum projections of z-stacks or focal plane stacks using Fiji[45] Simple Neurite Tracer with 3–10 neurite traces quantified. Maximum radial distance of neurite extension was recorded by one to two blinded observers as a straight-line measurement from the distal neurite end to the closest edge of the DRG body or to the edge of the inner gel as determined by transmitted light images (Fig. 1E). The number of neurites and groups of neurites crossing the interface from the outer gel into the

inner gel was counted by two blinded observers. DRGs without any discernible neurite growth were withdrawn from the analysis.

Statistics

All statistical analyses were performed using Prism 7 (GraphPad, San Diego, CA). For rheology storage and loss moduli (n = a minimum of three samples of each gel composition and NP tissue), metabolic activity (n = 5 experiments, triplicate wells for each group), and cell viability (n = 3 experiments, triplicate gels for each gel type, triplicate locations within each gel) significance was determined via two-way analysis of variance (ANOVA) and Tukey's multiple comparisons tests with significance threshold $p < 0.05$. Analysis of quantified neurites was performed using one-way ANOVA with Tukey's multiple comparisons tests for Figures 4, 6, and Supplementary Figure S1 and using unpaired two-tailed t tests for Figure 5 with $p < 0.05$ significance threshold for all analyses.

RESULTS

Fabrication and Characterization of Methacrylated Biomaterials

MAHA, MACS-A, and MACS-C exhibited consistent and robust methacrylation as assessed by proton NMR. Representative NMR spectra for MAHA (Fig. 2A), MACS-A (Fig. 2B), and MACS-C (Fig. 2C) are shown. Batches of MAHA consistently exhibited a 1.09 ± 0.053 degree of methacrylation (n = 5 batches), while MACS-A had a 1.50 ± 0.029 degree of methacrylation (n = 3), and MACS-C had a 1.19 ± 0.137 degree of methacrylation (n = 2).

Mechanical Characterization of Hydrogels

The physical properties of all hydrogels were investigated using rheology (Fig. 2D). The storage modulus was slightly increased in gels containing MACS-A or MACS-C compared with gels containing MAHA alone (Fig. 2E). Increases in storage modulus of the same magnitude as observed with the CS biomaterials were reproduced in MAHA-only gels by increasing the MAHA concentration (Supplementary Fig. S1F). The storage moduli of the base MAHA hydrogels and MAHA/MACS-A gels were on the same order of magnitude as that of NP tissue explants, and the loss moduli for the gels and NP had greater variability but were all of a similar order of magnitude (Fig. 2E–F).

Verification of Cytocompatibility of Base Hydrogels with NP Cells

Since the intended use of these biomaterials is in disc therapeutics or replacements, the cytocompatibility of the biomaterials with NP cells was investigated via metabolic activity over time (Fig. 3A). The addition of MACS-A or MACS-C to the hydrogel was compared with a control MAHA-only gel. There were no statistically significant differences between the metabolic activities of NP cells in the different gel types on the same day in culture, but there were significant increases in metabolic activity over time within each gel type ($p < 0.05$). The ratio of living to dead cells at the end of the 7-day culture period was quantified using confocal fluorescence microscopy (Fig. 3B). The mean percent live cells per region of interest was slightly larger in the MAHA/MACS-A hydrogels than in the MAHA-only or MAHA/MACS-C gels ($p < 0.05$). Representative confocal fluorescent images of NP cells in hydrogels are presented with live/dead staining (Fig. 3C–E).

Determination of Neuroinhibition in Uniform 3D Hydrogels

Degree of neuroinhibition was established by measuring the neurite length and radial extension from the DRG body in immunofluorescence images in which neurofilament H was stained to visualize the neuronal cytoskeleton morphology. Since all pre-existing neurites outside of the DRG were removed prior to embedding, the distance of neurite extension into the surrounding gel indicates whether the hydrogel is permissive or inhibitory for neurite growth. The images of the DRGs are presented as inverted, grayscale images of the fluorescent signal to allow better visualization of the fine detail of the neurites. Representative examples of DRGs in an MAHA hydrogel (Fig. 4A), an MAHA/MACS-A hydrogel (Fig. 4B), and an MAHA/MACS-C hydrogel (Fig. 4C) are shown. Graphs of the distributions of traced neurite lengths (Fig. 4D) and the radial distance of neurite extension from the DRG (Fig. 4E) demonstrate that MACS-A significantly inhibited neurite growth by both measures ($p < 0.05$) and that MACS-C significantly inhibited the maximum radial length of neurite extension ($p < 0.05$) but not traced neurite length. As the neuroinhibitory properties of the MACS-A biomaterial were greater than those of MACS- C, MACS-A was utilized for the in vitro disc innervation model.

Since the physical properties of hydrogels containing CS biomaterials exhibited increased hydrogel stiffness (Fig. 2), the neurite growth of DRGs was examined in gels containing increased concentrations of MAHA to mimic the higher storage moduli seen in MAHA/MACS- A and MAHA/MACS-C gels (Fig. 2 and Supplementary Fig. S1). These data demonstrate that increased MAHA concentration promoted neurite growth rather than inhibiting it ($p < 0.05$). Therefore, the neuroinhibitory properties of the CS biomaterials are not due to increased hydrogel stiffness.

Development and Characterization of In Vitro Disc Innervation Culture Model

Using the novel in vitro model of disc innervation, the neuroinhibitory capacity of a CS biomaterial was screened using an MACS-A core (disc mimic) and an MAHA-only outer gel (Fig. 1D). Representative inverted-fluorescence images of DRGs growing across gel interfaces with a neuro-permissive MAHA inner gel (Fig. 5A) and with a neuroinhibitory MACS-A inner gel (Fig. 5B) are shown in grayscale to better visualize fine neurites. The ability of the MACS-A biomaterial to inhibit neurite extension across the hydrogel interface was assessed by measuring the traced length of neurites from the border of the inner gel (Fig. 5C), the straight-line/radial extension of the neurites into the inner gel (Fig. 5D), and the total number of neurites or groups of neurites crossing the outer/inner gel interface (Fig. 5E). The MAHA/MACS-A hydrogels were significantly more neuroinhibitory than MAHA-only hydrogels by all three measures of neurite growth ($p < 0.05$).

To confirm that the neuroinhibitory effects of MACS-A were due to the CS itself, chondroitinase ABC enzymatic digestion of the inner gels was performed prior to DRG embedding. Representative images of DRGs growing across gel interfaces with a digested MAHA inner gel (Fig. 6A), an undigested MAHA/MACS-A inner gel (Fig. 6B), and a digested MAHA/MACS-A inner gel (Fig. 6C) are shown. Neurite growth was quantified by the traced length of neurites from the border of the inner gel (Fig. 6D), the straight-line/radial extension of the neurites into the inner gel (Fig. 6E), and the total number of neurites

or groups of neurites crossing the outer/inner gel interface (Fig. 6F). Neurite growth into the digested MAHA/MACS-A gel was significantly greater than the growth into the undigested MAHA/MACS-A gel ($p < 0.05$).

However, growth into the digested MAHA/MACS-A gel was slightly less than growth into the MAHA gel ($p < 0.05$), indicating partial rescue of the MACS-A neuroinhibition.

DISCUSSION

The novel disc innervation model presented here is a 3D hydrogel mimic of the interface between disc tissue and an external environment containing sensory nerves. Neuroinhibitory properties of biomaterials intended to treat disc degeneration and discogenic pain can be assessed using this model. The benefits of this 3D model over the assessment of neuroinhibitory properties of biomaterials in 2D culture include the control of mechanical properties which can influence cell phenotype[44] and neurite growth,[46] a more physiologically relevant topography in which neurites can branch in 3D, and a distinct interface between a neurite growth-permissive environment and a neuroinhibitory disc mimic. Another variation of a 3D culture system is an organ culture model in which actual disc tissue is cultured adjacent to a DRG; however, an organ culture is not well suited for screening the neuroinhibitory properties of specific biomaterials as there is much less control over the contents of the disc tissue and the individual disc samples will have increased variability compared with a hydrogel. In future experiments, other variables relevant to the healthy or degenerated disc microenvironment such as pH, signaling molecules, inflammatory cytokines, and oxidative stress can be controlled to assess their effects on sensory neurons interacting with the disc.[8]

Currently, researchers have developed many biomaterials that restore disc mechanical properties/height[47] or even prevent discogenic pain,[26] and our in vitro model could be utilized with those biomaterials to determine neuroinhibitory properties and mechanisms of neuroinhibition. Our model could also be adapted to test engineered biomaterials for therapeutic uses in which neurite growth is desired such as nerve or spinal cord injury and regeneration. Neuromodulation and targeted innervation can have widespread clinical impacts for neuropathy and pain, and this model provides a valuable way to assess the neuromodulatory properties of biomaterials.

The in vitro disc innervation model was utilized to screen the neuroinhibitory capacity of CS biomaterials for future use in therapeutics for discogenic pain. The data support the disc-like properties and NP cell compatibility of the biomaterials tested (Figs. 2 and 3). The hydrogel stiffness as indicated by the storage modulus was increased either by the incorporation of CS biomaterials or by increasing the concentration of MAHA, but increased MAHA concentrations actually promoted neurite growth so an increase in hydrogel stiffness was not sufficient to inhibit neurite growth (Supplementary Fig. S1). Published research demonstrates that neurite growth is dependent on hydrogel mechanical properties with substantially increased stiffness correlating with decreased nerve growth, but small variations (less than an order of magnitude) in stiffness do not yield significant growth differences.[46,48] The neuroinhibitory efficacy results for biomaterials containing the two

types of CS that are most physiologically relevant to the disc, CS-A and CS-C, support the conclusion that CS-A inhibits neurite growth both in a uniform gel and at an interface, while CS-C is less neuroinhibitory in the context of this model (Figs. 4–6).

The greater neuroinhibitory effects of CS-A than CS-C on rat DRG neurons in this model are consistent with neuroinhibition research in neonatal mouse cerebellar granule neurons,[40] but the opposite was found in a study on embryonic rat cortical neurons in which CS-C was more neuroinhibitory than CS-A.[41] These differences are likely because neurite growth response depends on the neuronal cell type and the local microenvironment, as the various CS types can bind to different neuronal receptors or sequester soluble signaling molecules.[49,50] Thus, the incorporation of biomaterials containing CS-A may improve the function of novel discogenic pain therapeutics by preventing neurite invasion from DRGs in a rat model, and the response of human DRG neurons to CS-A must be confirmed prior to clinical translation.

In addition to the direct neuroinhibitory effects of CS-A, there are other potential benefits to this molecule as a biomaterial. The vascularization of painful, degenerate discs allows increased immune cell infiltration which further exacerbates the inflammatory environment of the disc.[51] The human disc CSPG aggrecan and purified CS have been demonstrated to be anti-angiogenic either by direct effects on endothelial cell migration/adhesion or by decreasing the expression of angiogenic factors in chondrocytes.[13,52] Additionally, if incorporated into a therapeutic that includes mesenchymal stem cells, CS biomaterials could prevent angiogenic and neurotrophic paracrine signaling from the stem cells.[53]

The demonstration of neuroinhibition by CS-A in this model is a proof of principle and first step toward clinical translation. Many other steps on that path remain, such as engineering and validating a delivery method, animal model testing, and corroboration of neuroinhibition for human sensory neurons. One limitation of this model may be the use of neonatal rat DRGs. Neonatal DRGs were utilized for higher through-put, but the neuroinhibitory properties of MACS-A may need to be confirmed using adult rat DRGs prior to in vivo animal model use. Additionally, as there can be species-specific neuromodulatory responses to some types of CS, neuroinhibition screening using human DRGs will be necessary prior to clinical translation. Other biomaterial properties such as lack of immunogenicity must also be confirmed prior to intervention delivery. Importantly, the neuroinhibition of CS-A acts to prevent neurite growth into tissue but would not eliminate existing sensory neurites in a disc as a stand-alone biomaterial. Therefore, novel therapeutics must include other components to cause neurite dieback/removal or inhibit sensory neurite function in order to treat discogenic pain.

CONCLUSIONS

The in vitro disc innervation model presented here is a screening tool that can assess neuroinhibition at an interface for any biomaterial that can be incorporated or immobilized into a hydrogel, and this has widespread potential applications both for discogenic pain treatments and other conditions in which control of nerve growth is needed. The initially

screened CS biomaterials suggest that CS-A is a strong candidate for disc therapeutics as an NP cell compatible means to prevent disc innervation and discogenic pain.

Supplementary Material

Refer to Web version on PubMed Central for supplementary material.

ACKNOWLEDGMENTS

We would like to thank USMARC and Dr. Jeremy Miles for supplying porcine tissue, the Nano-Engineering Research Core Facility for confocal microscope support, the Research Instrumentation Facility and Dr. Martha Morton for assistance in acquiring NMR spectroscopy data, Alissa Zeitelhack for acquiring porcine nucleus pulposus tissue rheology data, and the Nebraska Center for Integrated Biomolecular Communication (NIH National Institutes of General Medical Sciences P20-GM113126) for funding this research.

REFERENCES

1. Andersson GB. 1999 Epidemiological features of chronic low-back pain. Lancet 354:581–585. [PubMed: 10470716]
2. Shmagel A, Foley R, Ibrahim H. 2016 Epidemiology of chronic low back pain in US adults: Data from the 2009-2010 National Health and Nutrition Examination Survey. Arthritis Care Res (Hoboken) 68:1688–1694. [PubMed: 26991822]
3. Meucci RD, Fassa AG, Faria NM. 2015 Prevalence of chronic low back pain: systematic review. Rev Saude Publica 49:49. [PubMed: 26270011]
4. Hoy D, Bain C, Williams G, et al. 2012 A systematic review of the global prevalence of low back pain. Arthritis Rheum 64: 2028–2037. [PubMed: 22231424]
5. DePalma MJ, Ketchum JM, Saullo T. 2011 What is the source of chronic low back pain and does age play a role? Pain Medicine 12:224–233. [PubMed: 21266006]
6. Manchikanti L, Jasper J, Singh V. 2001 Evaluation of the relative contributions of various structures in chronic low back pain. Spine 26:2641–2643. [PubMed: 11725251]
7. Schwarzer AC, Aprill CN, Derby R, et al. 1995 The prevalence and clinical features of internal disc disruption in patients with chronic low back pain. Spine 20:1878–1883. [PubMed: 8560335]
8. Fujii K, Yamazaki M, Kang JD, et al. 2019 Discogenic back pain: literature review of definition, diagnosis, and treatment. JBMR Plus 3:e10180.
9. Ashworth J, Green DJ, Dunn KM, et al. 2013 Opioid use among low back pain patients in primary care: is opioid prescription associated with disability at 6-month follow-up? Pain 154:1038–1044. [PubMed: 23688575]
10. Foster NE, Anema JR, Cherkin D, et al. 2018 Prevention and treatment of low back pain: evidence, challenges, and promising directions. Lancet 391:2368–2383. [PubMed: 29573872]
11. Chou R, Qaseem A, Snow V, et al. 2007 Diagnosis and treatment of low back pain: a joint clinical practice guideline from the American College of Physicians and the American Pain Society. Ann Intern Med 147:478–491. [PubMed: 17909209]
12. Johnson WEB, Caterson B, Eisenstein SM, et al. 2002 Human intervertebral disc aggrecan inhibits nerve growth in vitro. Arthritis Rheum 46:2658–2664. [PubMed: 12384924]
13. Johnson WEB, Caterson B, Eisenstein SM, et al. 2005 Human intervertebral disc aggrecan inhibits endothelial cell adhesion and cell migration in vitro. Spine 30: 1139–1147. [PubMed: 15897827]
14. Wang Y, Battié MC. 2014 Epidemiology of lumbar disc degeneration In: Shapiro IM, Risbud MV, editors. The intervertebral disc. Vienna: Springer p 139–156.
15. García-Cosamalón J, del Valle ME, Calavia MG, et al. 2010 Intervertebral disc, sensory nerves and neurotrophins: who is who in discogenic pain? J Anat 217:1–15. [PubMed: 20456524]
16. LA Binch A, Cole AA, Breakwell LM, et al. 2014 Expression and regulation of neurotrophic and angiogenic factors during human intervertebral disc degeneration. Arthritis Res Ther 16:416. [PubMed: 25209447]

17. Binch ALA, Cole AA, Breakwell LM, et al. 2015 Nerves are more abundant than blood vessels in the degenerate human intervertebral disc. Arthritis Res Ther 17:370. [PubMed: 26695177]
18. Coppes MH, Marani E, Thomeer RTWM, et al. 1990 Innervation of annulus fibrosis in low back pain. Lancet 336: 189–190.
19. Coppes MH, Marani E, Thomeer RTWM, et al. 1997 Innervation of “painful” lumbar discs. Spine 22:2342–2349. [PubMed: 9355214]
20. Freemont A, Peacock T, Goupille P, et al. 1997 Nerve ingrowth into diseased intervertebral disc in chronic back pain. Lancet 350:178–181. [PubMed: 9250186]
21. Peng B, Wu W, Hou S, et al. 2005 The pathogenesis of discogenic low back pain. J Bone Joint Surg Br 87b:62–67.
22. Ozawa T, Ohtori S, Inoue G, et al. 2006 The degenerated lumbar intervertebral disc is innervated primarily by peptide-containing sensory nerve fibers in humans. Spine 31:2418–2422. [PubMed: 17023849]
23. Wu B, Yang L, Peng B. 2019 Ingrowth of nociceptive receptors into diseased cervical intervertebral disc is associated with discogenic neck pain. Pain Med 20:1072–1077. [PubMed: 30848823]
24. Sainoh T, Sakuma Y, Miyagi M, et al. 2014 Efficacy of anti-nerve growth factor therapy for discogenic neck pain in rats. Spine 39:E757–E762. [PubMed: 24732837]
25. Miyagi M, Millecamps M, Danco AT, et al. 2014 ISSLS Prize winner: increased innervation and sensory nervous system plasticity in a mouse model of low back pain due to intervertebral disc degeneration. Spine 39:1345–1354. [PubMed: 24718079]
26. Mohd Isa IL, Abbah SA, Kilcoyne M, et al. 2018 Implantation of hyaluronic acid hydrogel prevents the pain phenotype in a rat model of intervertebral disc injury. Sci Adv 4:eaaq0597.
27. Shi C, Das V, Li X, et al. 2018 Development of an in vivo mouse model of discogenic low back pain. J Cell Physiol 233: 6589–6602. [PubMed: 29150945]
28. Vincent K, Mohanty S, Pinelli R, et al. 2019 Aging of mouse intervertebral disc and association with back pain. Bone 123: 246–259. [PubMed: 30936040]
29. Wachs RA, Hoogenboezem EN, Huda HI, et al. 2017 Creation of an injectable in situ gelling native extracellular matrix for nucleus pulposus tissue engineering. Spine J 17:435–444. [PubMed: 27989725]
30. Bowles RD, Setton LA. 2017 Biomaterials for intervertebral disc regeneration and repair. Biomaterials 129:54–67. [PubMed: 28324865]
31. Brown JM, Xia J, Zhuang B, et al. 2012 A sulfated carbohydrate epitope inhibits axon regeneration after injury. Proc Natl Acad Sci U S A 109:4768–4773. [PubMed: 22411830]
32. Jin J, Tilve S, Huang Z, et al. 2018 Effect of chondroitin sulfate proteoglycans on neuronal cell adhesion, spreading and neurite growth in culture. Neural Regen Res 13:289–297. [PubMed: 29557379]
33. Gilbert RJ, McKeon RJ, Darr A, et al. 2005 CS-4,6 is differentially upregulated in glial scar and is a potent inhibitor of neurite extension. Mol Cell Neurosci 29:545–558. [PubMed: 15936953]
34. Yu XJ, Bellamkonda RV. 2001 Dorsal root ganglia neurite extension is inhibited by mechanical and chondroitin sulfaterich interfaces. J Neurosci Res 66:303–310. [PubMed: 11592128]
35. Martins DE, Medeiros VP, Wajchenberg M, et al. 2018 Changes in human intervertebral disc biochemical composition and bony end plates between middle and old age. PLoS One 13:e0203932.
36. Dickendesher TL, Baldwin KT, Mironova YA, et al. 2012 NgR1 and NgR3 are receptors for chondroitin sulfate proteoglycans. Nat Neurosci 15:703–712. [PubMed: 22406547]
37. Mikami T, Yasunaga D, Kitagawa H. 2009 Contactin-1 is a functional receptor for neuroregulatory chondroitin sulfate-E. J Biol Chem 284:4494–4499. [PubMed: 19075012]
38. Shen Y, Tenney AP, Busch SA, et al. 2009 PTP sigma is a receptor for chondroitin sulfate proteoglycan, an inhibitor of neural regeneration. Science 326:592–596. [PubMed: 19833921]
39. Bayliss MT, Osborne D, Woodhouse S, et al. 1999 Sulfation of chondroitin sulfate in human articular cartilage. The effect of age, topographical position, and zone of cartilage on tissue composition. J Biol Chem 274:15892–15900. [PubMed: 10336494]

40. Wang H, Katagiri Y, McCann TE, et al. 2008 Chondroitin-4-sulfation negatively regulates axonal guidance and growth. J Cell Sci 121:3083–3091. [PubMed: 18768934]
41. Butterfield KC, Conovaloff A, Caplan M, et al. 2010 Chondroitin sulfate-binding peptides block chondroitin 6-sulfate inhibition of cortical neurite growth. Neurosci Lett 478:82–87. [PubMed: 20450957]
42. Smeds KA, Grinstaff MW. 2001 Photocrosslinkable polysaccharides for in situ hydrogel formation. J Biomed Mater Res 54:115–121. [PubMed: 11077410]
43. Nettles DL, Vail TP, Morgan MT, et al. 2004 Photocrosslinkable hyaluronan as a scaffold for articular cartilage repair. Annals of Biomedical Engineering 32:391–397. [PubMed: 15095813]
44. Seidlits SK, Khaing ZZ, Petersen RR, et al. 2010 The effects of hyaluronic acid hydrogels with tunable mechanical properties on neural progenitor cell differentiation. Biomaterials 31:3930–3940. [PubMed: 20171731]
45. Schindelin J, Arganda-Carreras I, Frise E, et al. 2012 Fiji: an open-source platform for biological-image analysis. Nat Methods 9:676–682. [PubMed: 22743772]
46. Willits RK, Skornia SL. 2012 Effect of collagen gel stiffness on neurite extension. J Biomater Sci Polym Ed 15:1521–1531.
47. Bowles RD, Gebhard HH, Härtl R, et al. 2011 Tissueengineered intervertebral discs produce new matrix, maintain disc height, and restore biomechanical function to the rodent spine. Proc Natl Acad Sci U S A 108:13106–13111. [PubMed: 21808048]
48. Balgude A 2001 Agarose gel stiffness determines rate of DRG neurite extension in 3D cultures. Biomaterials 22: 1077–1084. [PubMed: 11352088]
49. Miller GM, Hsieh-Wilson LC. 2015 Sugar-dependent modulation of neuronal development, regeneration, and plasticity by chondroitin sulfate proteoglycans. Exp Neurol 274: 115–125. [PubMed: 26315937]
50. Mizumoto S, Yamada S, Sugahara K. 2015 Molecular interactions between chondroitin-dermatan sulfate and growth factors/receptors/matrix proteins. Curr Opin Struct Biol 34:35–42. [PubMed: 26164146]
51. Doita M, Kanatani T, Harada T, et al. 1996 Immunohistologic study of the ruptured intervertebral disc of the lumbar spine. Spine 21:235–241. [PubMed: 8720410]
52. Calamia V, Lourido L, Fernández-Puente P, et al. 2012 Secretome analysis of chondroitin sulfate-treated chondrocytes reveals anti-angiogenic, anti-inflammatory and anti-catabolic properties. Arthritis Res Ther 14:R202. [PubMed: 23031212]
53. Wood CR, Al Delfi IRT, Innes JF, et al. 2018 Exposing mesenchymal stem cells to chondroitin sulphated proteoglycans reduces their angiogenic and neuro-adhesive paracrine activity. Biochimie 155:26–36. [PubMed: 29680669]

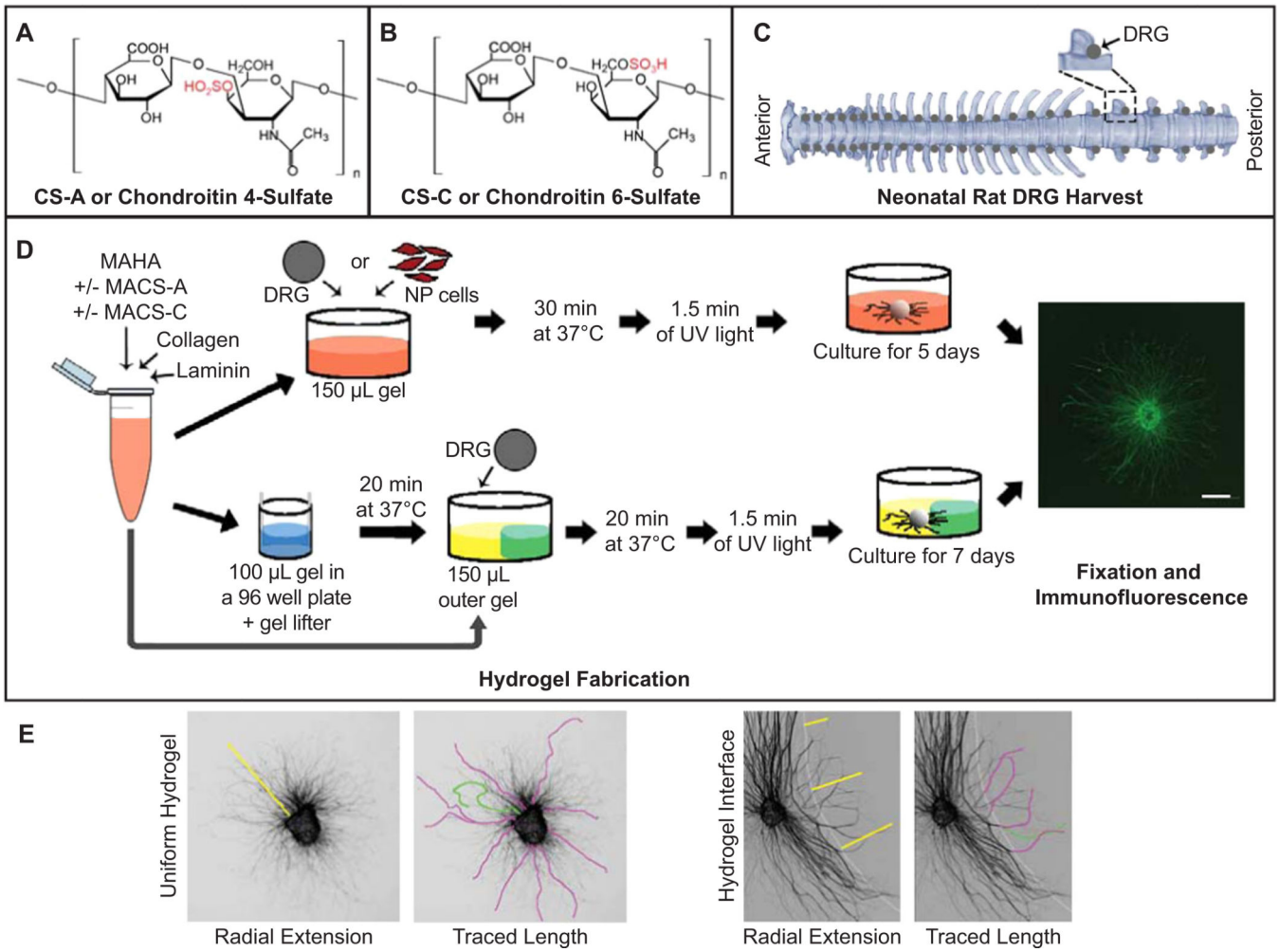

Figure 1.

Schematic of experimental design and in vitro model fabrication. The structure of chondroitin-4-sulfate (CS-A) (A) and chondroitin-6-sulfate (CS-C) (B) are shown with the sulfate group in red. The locations of the neonatal dorsal root ganglion (DRG) harvested for these experiments are indicated in (C). The process of hydrogel fabrication in (D) depicts the differences between making a uniform composition hydrogel for either nucleus pulposus (NP) encapsulation or for DRG embedding versus making the in vitro disc innervation model with an inner gel and outer gel to embed a DRG at the hydrogel interface. Examples of the two different types of neurite growth quantification, traced neurite length (purple and green traces, green indicating the longest trace) and radial neurite extension (yellow line), are shown in (E) with the white line on the hydrogel interface images indicating the interface between the inner and outer gels. MACS-A, methacrylated CS-A; MACS-C, methacrylated CS-C; MAHA, methacrylated hyaluronic acid; UV, ultraviolet light. [Color figure can be viewed at wileyonlinelibrary.com]

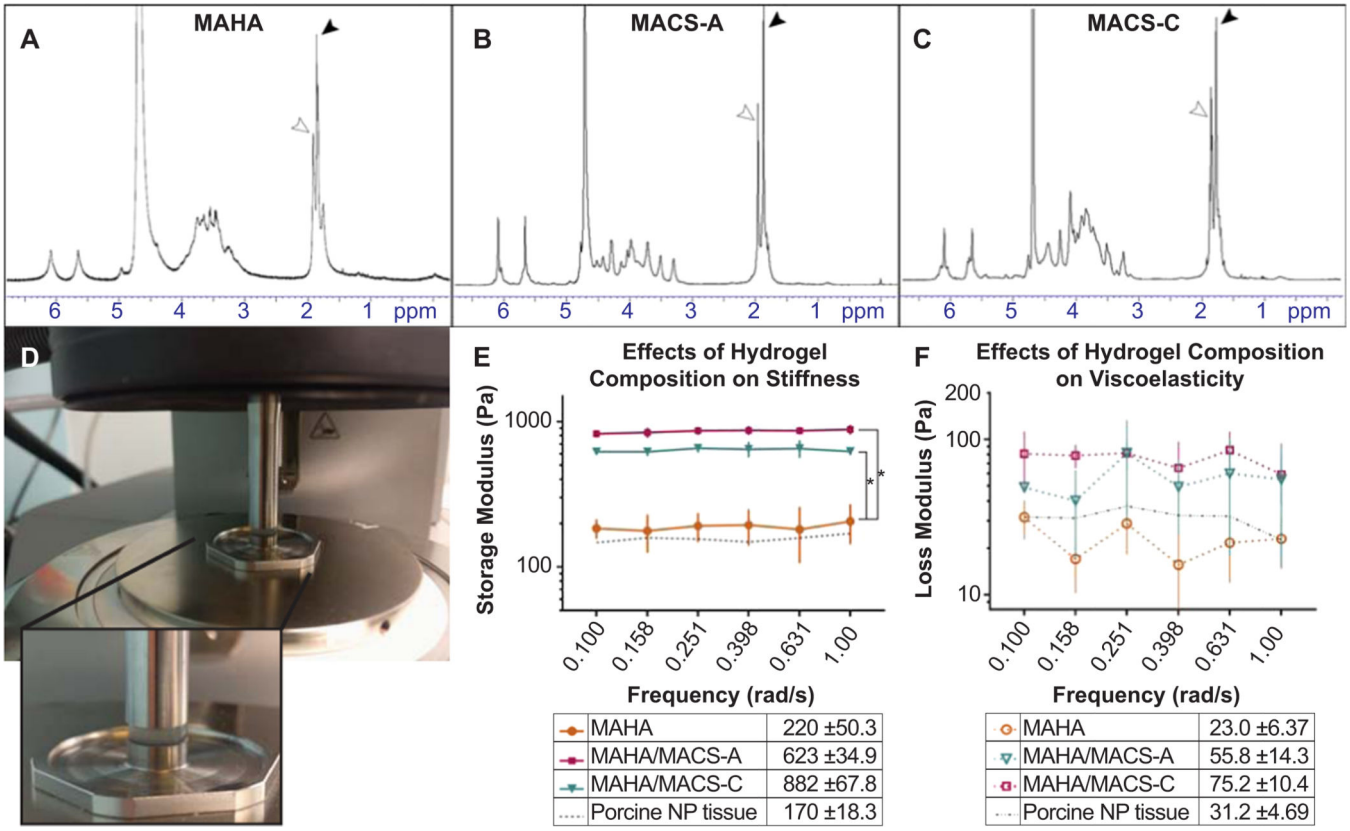

Figure 2.

Characterization of biomaterials and hydrogels. The methacrylated biomaterials and the hydrogels fabricated using those biomaterials were characterized by nuclear magnetic resonance (NMR) to quantify the degree of biomaterial methacrylation and by rheology to quantify the hydrogel mechanical properties. Representative proton NMR spectra for methacrylated hyaluronic acid (MAHA) (A), methacrylated chondroitin sulfate A (MACS-A) (B), and methacrylated chondroitin sulfate C (MACS-C) (C) are displayed. The degree of methacrylation was calculated as the ratio of the integral of the methacrylate peak at ~1.8 ppm (black arrowhead) to the integral of the hyaluronic acid or chondroitin sulfate peak at ~1.9 ppm (white arrowhead).[42,44] Oscillatory rheology was performed on hydrogels containing the methacrylated biomaterials and collagen, with the apparatus depicted in (D). The increase in mean storage modulus observed with the incorporation of MACS-A or MACS-C at 10 mg/ml into gels containing MAHA at 2.25 mg/ml ($n = 3$ for each group) is graphed in (E) and compared with the storage modulus of porcine nucleus pulposus (NP) tissue explants ($n = 5$). The storage moduli of MAHA gels and NP tissue are not significantly different, and the storage moduli of both MAHA/MACS-A and MAHA/MACS-C gels are significantly greater than those of MAHA gels or NP tissue ($p < 0.05$). The loss moduli for the gels and NP tissue are graphed in (F), and no consistent statistical differences were observed. Error bars are standard deviation of the mean. [Color figure can be viewed at wileyonlinelibrary.com]

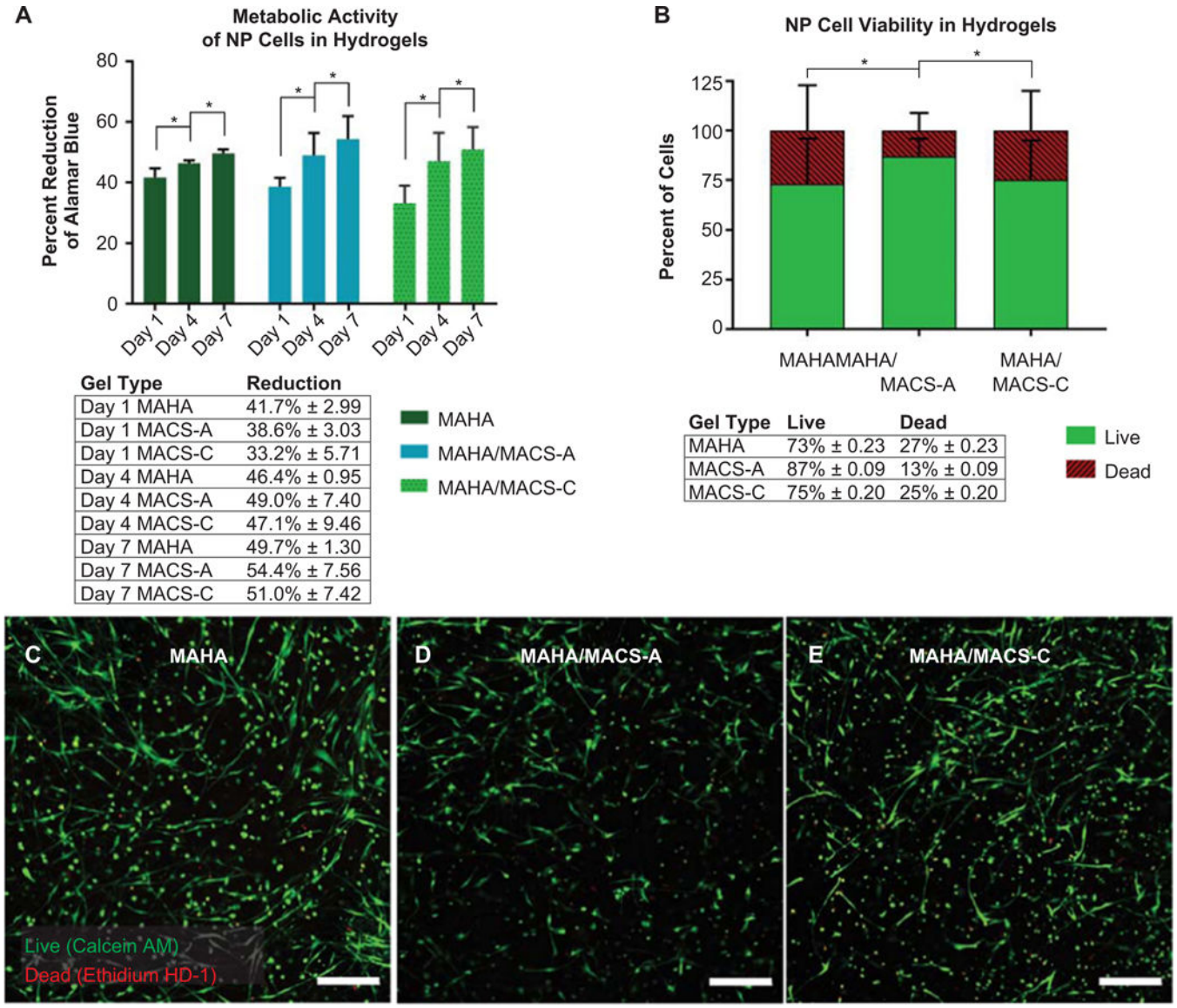

Figure 3.

Cytocompatibility of hydrogels with human nucleus pulposus (NP) cells. The metabolic activity of human NP cells cultured in 3D hydrogels was quantified by the reduction of alamarBlue in culture media at Days 1, 4, and 7 in culture ($n = 5$ experiments, triplicate wells for each group) (A). There was no difference in metabolic activity between hydrogel types on the same day in culture, but there was an increase in metabolic activity over time for each hydrogel group (*$p < 0.05$; error bars are standard deviation of the mean). The viability of NP cells at the end of Day 7 ($n = 3$ experiments, triplicate wells for each group, triplicate regions of interest imaged per gel) was quantified from live/dead fluorescence staining and confocal microscopy (B). The mean percent of live cells (green) was greater for the methacrylated hyaluronic acid (MAHA)/methacrylated chondroitin-4-sulfate (MACS-A) gels than for the MAHA and MAHA/methacrylated chondroitin-6-sulfate (MACS-C) gels (*$p < 0.05$; error bars are standard deviation of the mean). Representative live/dead

fluorescent images from NP cells in MAHA gels (C), MAHA/MACS-A gels (D), and MAHA/MACS-C gels (E) are presented. Scale bars are 200 μm. [Color figure can be viewed at wileyonlinelibrary.com]

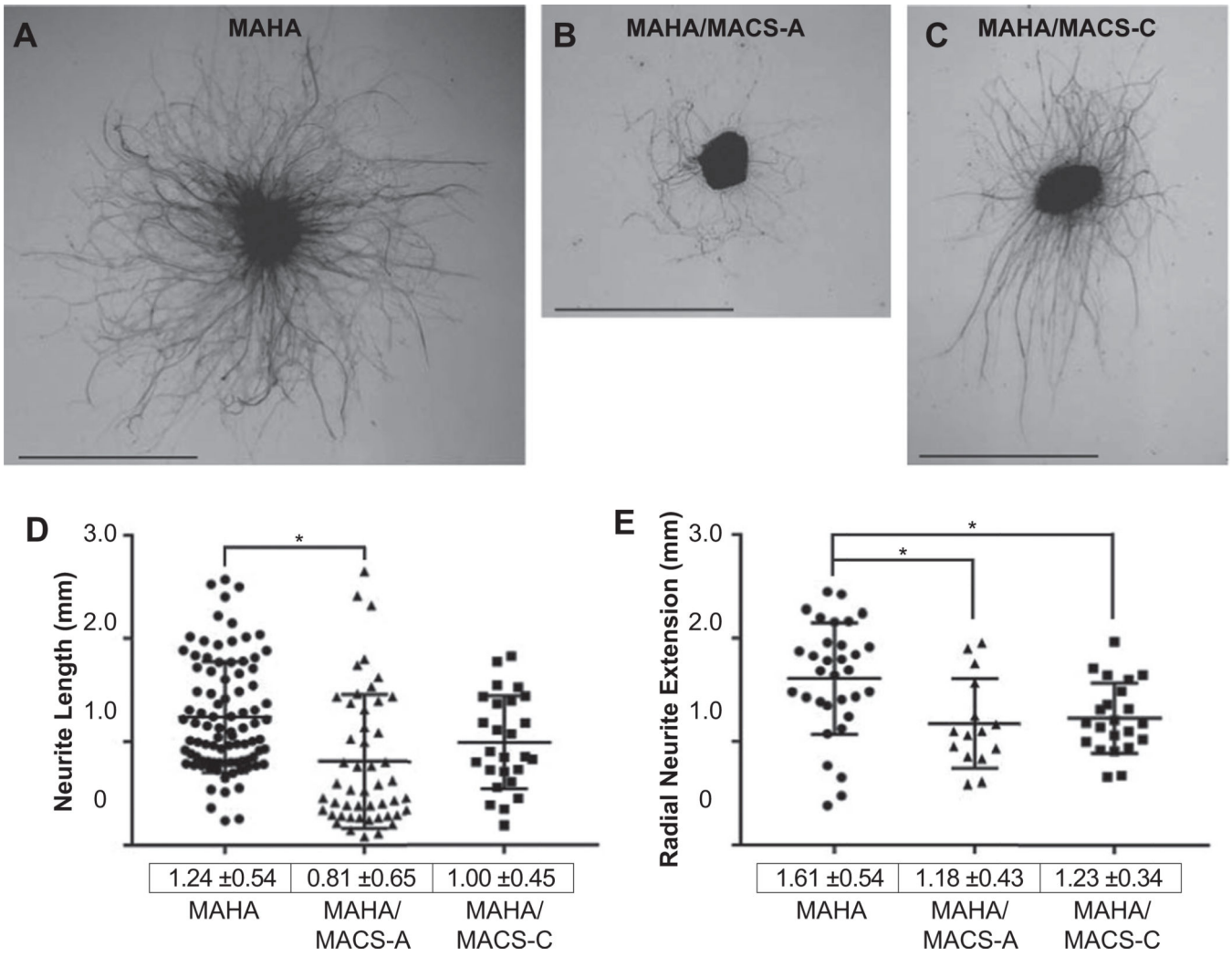

Figure 4.

Neurite growth inhibition by chondroitin sulfate biomaterials. Representative inverted-fluorescence image projections stained against neurofilament H (NF-H) show the growth of neurites from the original dorsal root ganglion (DRG) cell body cluster in hydrogels containing 2.5 mg/ml methacrylated hyaluronic acid (MAHA) (A), 2.25 mg/ml MAHA plus 10 mg/ml methacrylated chondroitin-4-sulfate (MACS-A) (B), and 2.25 mg/ml MAHA plus 10 mg/ml methacrylated chondroitin-6-sulfate (MACS-C) (C). Scale bars are 2 mm. Quantified traced neurite lengths (D) and radial distance of neurite extension from the DRG body (E) demonstrate inhibition of neurite growth by MACS-A via both measures and by MACS-C in radial distance only (*$p < 0.05$; error bars are standard deviation of the mean). Neurite lengths are quantified in 90 DRGs across 10 experiments for MAHA gels, in 49 DRGs in eight experiments for MAHA/MACS-A gels, and in 26 DRGs from three experiments for MAHA/MACS-C gels. Radial distance is quantified from three experiments with 32 DRGs in MAHA, 15 DRGs in MAHA/MACS-A, and 22 DRGs in MAHA/MACS-C gels.

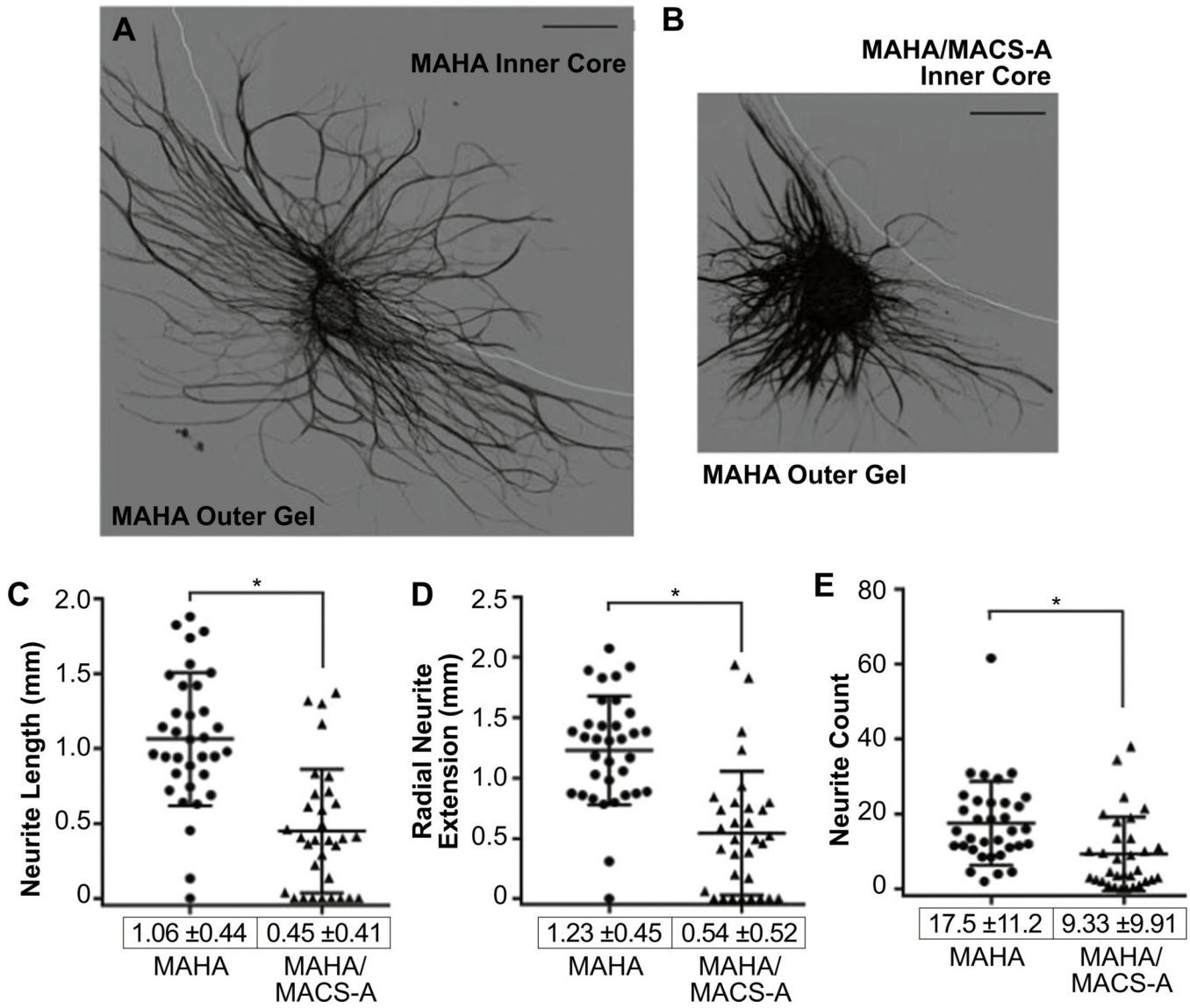

Figure 5.

Neurite growth inhibition at an interface by a chondroitin sulfate biomaterial. Representative inverted-fluorescence confocal maximum intensity z-stack projections from immunofluorescence staining against neurofilament H (NF-H) show the growth of neurites from the original dorsal root ganglion (DRG) cell body cluster. DRGs are embedded in a hydrogel containing 2.5 mg/ml methacrylated hyaluronic acid (MAHA) adjacent to either a hydrogel containing 2.5 mg/ml MAHA (A) or adjacent to a hydrogel containing 2.25 mg/ml MAHA plus 10 mg/ml methacrylated chondroitin-4-sulfate (MACS-A) (B). Scale bars are 0.5 mm. Neurite lengths and radial distance are measured from the edge of the inner core gel (white line; determined by transmitted light microscopy). Quantification of traced neurite lengths (C), radial distance of neurite extension into the inner core gel (D), and the number of neurites/groups of neurites crossing from the outer gel to the inner gel (E) demonstrate inhibition of neurite growth by MACS-A via all measures (*$p < 0.05$; error bars are standard deviation of the mean). Traced neurite lengths, radial neurite extension, and count of neurites

crossing the interface are quantified across three experiments from 34 DRGs with 2.5 mg/ml inner core MAHA gels and 32 DRGs with 2.25 mg/ml MAHA plus 10 mg/ml MACS-A inner core gels.

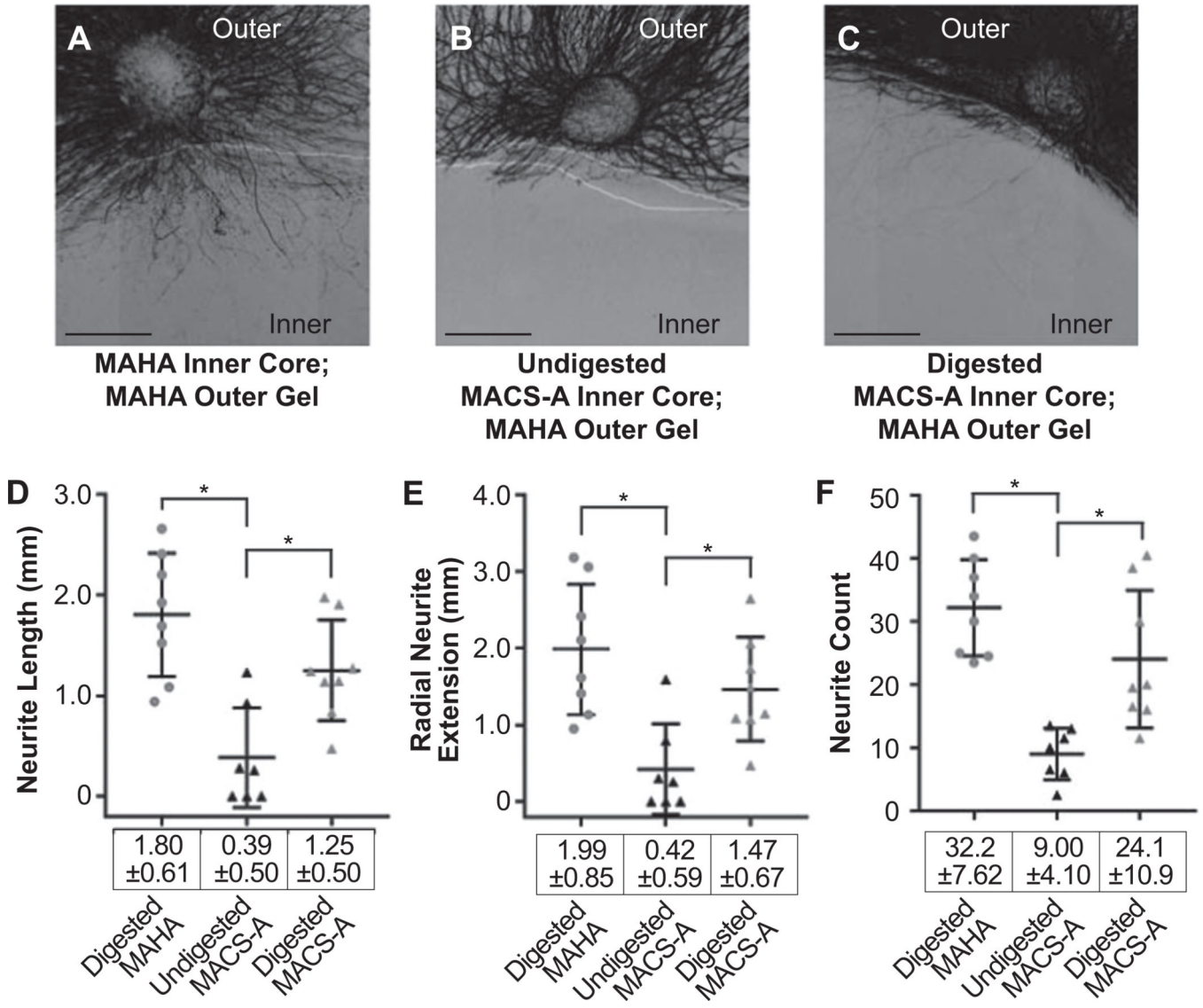

Figure 6.

Rescue of chondroitin sulfate neuroinhibition by enzymatic digestion. Representative inverted-fluorescence confocal z-stack projections stained for neurofilament H (NF-H) show the growth of neurites from the original dorsal root ganglion (DRG) cell body cluster. DRGs are embedded in a hydrogel containing 2.5 mg/ml methacrylated hyaluronic acid (MAHA) adjacent to a chondroitinase ABC digested hydrogel containing 2.5 mg/ml MAHA (A), an undigested hydrogel containing 2.25 mg/ml MAHA plus 10 mg/ml methacrylated chondroitin-4-sulfate (MACS-A) (B), or a chondroitinase ABC digested hydrogel containing 2.25 mg/ml MAHA plus 10 mg/ml MACS-A (C). Scale bars are 0.5 mm. Neurite lengths and radial distance are measured from the edge of the inner core gel (white line(s); determined by transmitted light microscopy). Quantification of traced neurite lengths (D), radial distance of neurite extension into the inner core gel (E), and the number of neurites/groups of neurites crossing from the outer gel to the inner gel (F) demonstrate that chondroitinase ABC digestion decreases the neuroinhibition of MACS-A because all three

neurite growth measurements are higher in the digested MAHA/MACS-A inner gels than in the undigested MAHA/MACS-A inner gels (*$p < 0.05$; error bars are standard deviation of the mean). Neurite growth into the digested MAHA inner gels is also significantly higher than growth in the undigested MAHA/MACS-A inner gels. Traced neurite lengths, radial neurite extension, and counts of neurites crossing the gel interface are quantified across two experiments from eight DRGs with digested inner core MAHA gels, seven DRGs with undigested inner core MAHA/MACS-A gels, and eight DRGs with digested inner core MAHA gels.